Modeling Metal Oxide Surge Arrester for the Modern Polarization Based Diagnostics

T. K. Saha
School of Information Technology and Electrical Engineering,
University of Queensland, Australia

and K. P. Mardira
Energy Australia, Newcastle, Australia

ABSTRACT

Recently a number of new non-destructive diagnostic techniques have been investigated for the reliable condition assessment of the ageing of metal oxide surge arrester (MOSA). Among them polarization/depolarization current and return voltage measurement techniques showed very promising results. This paper presents an insulation polarization model for investigating polarization-based diagnostics for metal oxide surge arrester. The simulations of the proposed model are validated and verified by comparing the data from the polarization/depolarization current measurements. The simulation of return voltage for MOSA is also performed to validate the insulation polarization model. Finally, the usefulness of this model for MOSA diagnostics has been highlighted in this paper.

Index Terms — **Metal oxide surge arrester, ageing and diagnostics, polarization/depolarization current, return voltage.**

1 INTRODUCTION

GAPLESS Metal Oxide Surge Arresters (MOSA) primary function is to protect all equipment in the system against various electrical overstress. It is known that current-voltage characteristics of metal oxide varistors become degraded due to the continuous application of ac or due to transients with currents larger than the varistors ratings. To test for any such degradation manufacturers normally apply single pulse 8/20 μs lightning transients at the rated current of the device. However, it is now known that most lightning ground flashes consist of multiple return strokes.

Many investigations of field aged cables and transformers have reported meaningful interpretations of the condition of the insulation by using new diagnostic techniques such as- return voltage measurement and polarization/depolarization current measurement. Since a MOSA is an insulator at normal conditions (below its rated voltage), the effect of polarization and depolarization of its dipole within the insulation can be monitored by any of these polarization-based diagnostics. These new diagnostic techniques have been successfully applied to a number of artificially degraded MOSA's and have been reported in a number of publications [1-4]. Results from these diagnostics cannot be interpreted confidently unless the exact relationship between the measured dielectric parameters and the fundamental dielectric processes of insulations is clearly understood.

Surge protection of transmission and distribution systems are commonly examined based on the results of their network simulation of their responses subject to different electrical overstress. Correct simulation needs an accurate model of the network elements and this necessitates an accurate model for Metal Oxide Surge Arrester (MOSA). The simulation of the dielectric processes gives the possibility to explain some exact relationships that may help to interpret the test results correctly. An effort has been made in this paper to understand the dielectric response of MOSA as related to its fundamental structure and its behavior to external electric field. A model of the insulation structure of MOSA based on the principles of linear dielectric response has been derived. The model presented here allows quantitative analysis of the dielectric response of a MOSA.

More specifically, the aim here is to determine the insulation equivalent model of MOSA, which could be useful to predict the degree of degradation. The simulations of the proposed models are validated using MATLAB based software. Effectiveness and accuracy of the proposed

Paper received on 23 November 2004, in final form 11 March 2005.

model are verified by comparing the data from the polarization/depolarization current measurement with the results from polarization model. The simulations of return voltage on the polarization models are also performed using MATLAB to validate the insulation polarization model. The effect of lightning current impulses on MOSA's polarization model is also discussed in this paper in detail.

2 THEORY

2.1 POLARIZATION/DEPOLARIZATION CURRENT [5]

Assuming a homogeneous electric field E(t) is applied to the dielectric material, the current density through the surface of the material can be written as

$$J_p(t) = \sigma E(t) + \varepsilon_0 \varepsilon_r \frac{dE(t)}{dt} + \varepsilon_0 \frac{d}{dt}\int_0^t f(t-\tau).E(\tau)d\tau \quad (1)$$

where σ is the dc conductivity, ε_o is the vacuum permittivity, ε_r is the relative permittivity of the insulation at power frequency and *f(t)* is the response function of the material. For a homogeneous material, the field strength *E(t)* can be considered as generated by an external voltage U(t), where E(t) = U(t)/meter(m). To convert current density to a current equation, E(t) in equation (1) is replaced by U(t)/m and equation (1) is multiplied by the geometric factor of the insulation structure. If the capacitor configuration consists of parallel plate electrodes of area A and spacing d sandwiching a dielectric of permittivity ε, the capacitance of the test object is given by equation (2)

$$C = (\varepsilon A/d) = (\varepsilon_r \varepsilon_o A/d) = \varepsilon_r(\varepsilon_o A/d) = \varepsilon_r C_g \quad (2)$$

where C_g = geometric capacitance = C/ε_r = (ε_o A/d) = ε_o (Geometric Factor); and geometric Factor = A/d = C_g/ε_o (unit m).

Then the polarization current is given by equation (3)

$$i_p(t) = C_g\left[\frac{\sigma}{\varepsilon_0}U(t) + \varepsilon_r \frac{dU(t)}{dt} + \frac{d}{dt}\int_0^t f(t-\tau).U(\tau)d\tau\right] \quad (3)$$

If the applied voltage is a step voltage as given in equation (4)

$$U(t) = \begin{cases} 0 & t < 0 \\ U_0 & 0 \le t \le t_c \\ 0 & t > t_c \end{cases} \quad (4)$$

This will give zero current for times before t = 0, and so-called polarization currents for times $0 \le t \le t_c$. Due to a constant step voltage, the displacement component of the current is zero. Hence, the polarization current is built up in two parts. One part is related to the conductivity of the test object and the other is related to the activation of the different polarization processes within the test object.

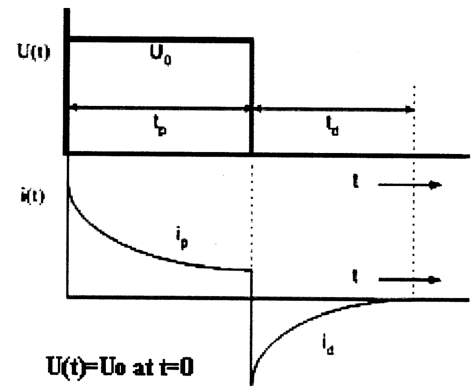

Figure 1. Polarization/depolarization current curves.

The polarization (charging) current through the object can thus be expressed as

$$i_p(t) = C_g U_0\left[\frac{\sigma}{\varepsilon_0} + f(t)\right] \quad (5)$$

Once the step voltage is replaced by a short circuit, a depolarization current builds up. The depolarization current is expressed as in equation (6). The process of polarization/depolarization is described in Figure 1.

$$i_d(t) = -C_g U_o\left[f(t) - f(t+t_p)\right] \quad (6)$$

It was found that the response function *f(t)* for the MOSA could be expressed in a general expression following the universal relaxation law as in equation (7), which is also found in many other experimental observations [6], where, m and n are constants.

$$f(t) = mt^{-n} \quad (7)$$

In order to estimate the dielectric response function *f(t)* from a depolarization current measurement it is assumed that the dielectric response function is a continuously decreasing function in time, then if the polarization period is sufficiently long, so that $f(t + t_p) \cong 0$, the dielectric response function *f(t)* is proportional to the depolarization current. Thus from equation (6), the dielectric response function *f(t)* can be approximated as in equation (8).

$$f(t) \approx \frac{-i_d(t)}{C_g U_o} \quad (8)$$

From the measurements of polarization and depolarization currents, it is possible to estimate the dc conductivity σ of a test object. If the test object is charged for a sufficiently long time so that $f(t + t_p) \cong 0$. Equations (5) and (6) can be combined to express the dc conductivity of the dielectric as

$$\sigma \approx \frac{\varepsilon_0}{C_g U_0}\left(i_p(t) - i_d(t)\right) \quad (9)$$

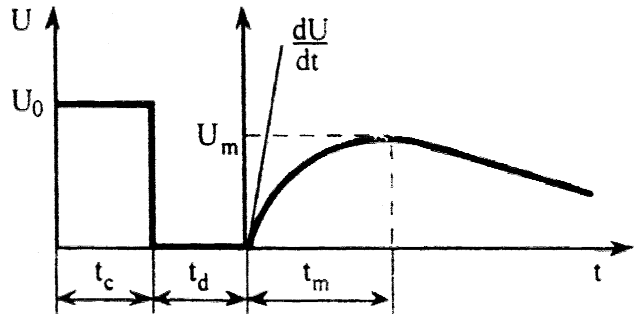

Figure 2. Return voltage phenomena.

2.2 RETURN OR RECOVERY VOLTAGE

The return voltage is based on the polarization and subsequent depolarization of dipoles within the insulating material as well as on the charging and discharging of grain boundaries and space charge effect [2]. Figure 2 shows the typical steps of a return voltage measurement.

The return voltage measurement comprises three steps:

• Charge the tested object for a pre-selected time (t_c) with a dc voltage (U_o), which is much lower than the rated voltage.

• Discharge the tested object for a short period (normally half of the charging time, $t_d = 0.5\ t_c$).

• Measure the open circuit voltage built up across the object (U_r).

Three important parameters may characterize the condition of insulation. They are maximum return voltage (U_{rmax}), time to reach maximum return voltage (central time constant (CTC- t_m) and the initial slope (slope of return voltage curve for first few seconds $S_r = du/dt$) [3, 4].

The polarization processes, which are not completely relaxed during the grounding period, will relax and give rise to a recovery voltage across the electrodes of the insulation. The current density during the return voltage measurement is zero and equation (10) gives the expression of current density. Where $E_r(t)$ is the electric field resulting from the return voltage build up U_r across the open circuited dielectric.

$$j(t) = \sigma E_r(t) + \varepsilon_0 \varepsilon_r \frac{d}{dt} E_r(t) + \varepsilon_0 \frac{d}{dt}\left\{\int_0^t f(t-\tau) E_r(\tau)\, d\tau\right\} \tag{10}$$

For $t_2 < t < \infty$, i.e. during the return voltage measurement period, the current is zero (open circuit condition of insulation) $i(t = t_2) = 0$. Also the current density j(t) being zero during the return voltage measurement. Equation (10) can be re-written as equation (11) and $E_r(t)$ can be numerically solved provided *f(t)* and the conductivity σ of the dielectric material are known.

$$j(t) = \sigma E_r(t) + \varepsilon_0 \varepsilon_r \frac{d}{dt} E_r(t) + \varepsilon_0 \frac{d}{dt}\left\{\int_{t_2}^t f(t-\tau) E_r(\tau)\, d\tau\right\} = 0 \tag{11}$$

If *f(t)* can be parametrised from the curve fitting of depolarisation current then conductivity can be estimated from equation (9). However, equation (11) can not be solved analytically and some numerical integration technique can be used for the return voltage estimation provided appropriate relative permittivity value of the metal oxide is accurately known. In reality, relative permittivity of the metal oxide can be only accurately estimated by frequency domain dielectric loss factor measurement. Hence, an alternate electrical circuit based model has been proposed to explain the polarization characteristics of transformer/cable dielectric materials by a number of researchers. This circuit based model has been applied in this paper to explain the MOSA characteristics due to the application of an external electric field.

3 POLARIZATION EQUIVALENT MODEL FOR METAL OXIDE SURGE ARRESTERS-DEBYE APPROACH

In the presence of an electric field, E, there are two main leakage current components that exist in a dielectric. They are conduction and polarization currents. The conduction and polarization currents both will be affected by any changes to the microstructure. The polarization current is due to the tendency of dipoles to align in the direction of the field.

The polarization process is described as a process of energy storage and only exists in the presence of an external field. When the field is removed, the dipoles relax and then return to the original state after a long time [12]. An insulation polarization model can be represented by an equivalent model comprising the insulation resistance and geometric capacitance with a number of additional R-C branches [8, 12], as shown in Figure 3. The parallel R-C branches represent the individual polarization processes with their time constants $R_{pn}\ C_{pn}$ and can be treated independent to each other. The representation of the polarization processes by parallel R-C branches allows following the theory of distributed relaxation times to predict the response of the insulation, which hardly follows ideal Debye behavior [6]. The number of branches in most practical modeling purposes varies from four to ten depending upon the nature of the depolarization current. The range of the values of the individual time constants, R_{pn} and C_{pn} are found to be dependent upon the insulation condition.

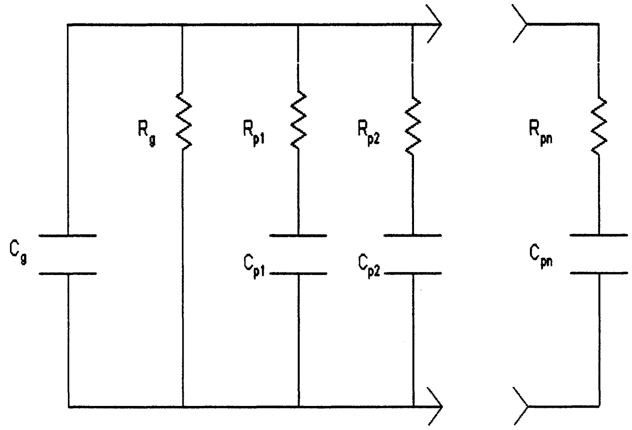

Figure 3. Equivalent circuit of insulation for polarization model.

The presence of the polarization introduces a permittivity ε_r in the field equation D $=$ ε_o ε_r E. The polarization is not observable but we can study its time development by measuring the current. The current density is the sum of the conduction and displacement currents. The conduction current in the insulation is due to a leakage or internal resistance R_g while the displacement current is due to the geometric capacitance C_g, internal resistance R_g and the pairs (R_{pn}, C_{pn}) with the associated time constant given by $\tau_n = R_{pn}C_{pn}$.

In this paper, an attempt is made to identify the polarization model of MOSA by means of polarization/depolarization current measurement. The aim is to investigate the MOSA polarization model parameters, which could be useful to determine the condition of its insulation after various electrical stresses particularly lightning impulse current pulses. The calculation of model parameters was performed using MATLAB.

4 IDENTIFICATION OF THE EQUIVALENT CIRCUIT USING - POLARIZATION CURRENTS AND DEPOLARIZATION CURRENTS

The polarization/depolarization currents are based on an application of a dc voltage to an insulator to establish polarization, and then the removal of the charging voltage to relax the dipoles (depolarization current). The equivalent polarization model can be identified by calculating the slope of depolarization current on each R-C branch and comparing it to the slope of the total depolarization current [9]. Figure 4 shows the polarization/depolarization current measurement set up on an insulation network.

During the application of dc voltage V across the dielectric for a pre-selected polarization time (t_c), in this case for up to 10,000 s with the switch closed in position 1 (as in Figure 4), the k-th capacitor C_{pk} is charged with a

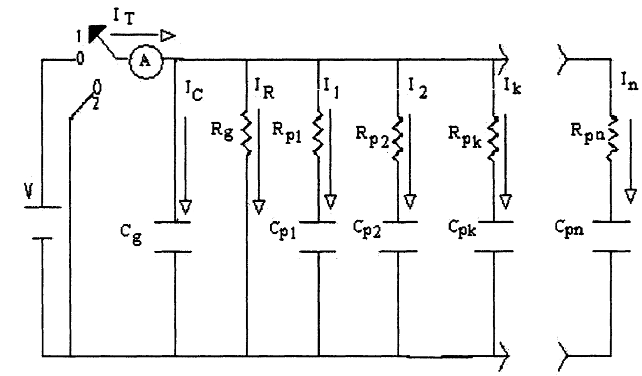

Figure 4. Polarization model for an insulation network.

final value given by equation (12)

$$V_{Cpk}\,(t_c) = V\left(1\text{−}\exp\left[-t_c/R_{pk}\,C_{pk}\right]\right) \tag{12}$$

The switch is then closed to position 2 at t $>$10000 seconds with pre-selected depolarization time (t_d) of 10,000 s. The corresponding depolarization branch current (I_{dk}) is given by

$$I_{dk}(t) = \frac{V_{Cpk}\exp\left(\dfrac{-(t-t_c)}{\tau_k}\right)}{R_{pk}} \tag{13}$$

where $\tau_k = R_{pk}\,C_{pk}$ is the individual elements ($R_{pk}-C_{pk}$) corresponding time constant. The total depolarisation current comprises of summation of various relaxation mechanisms that appears at different locations within the insulation. Various parts of the insulation have their unique relaxation characteristics depending upon the ageing condition. The relaxation or depolarization current can thus be modeled as the sum of exponentials of the various relaxation mechanisms.

$$I_{dT}(t) = \sum_{k=1}^{n} I_{dk}(t) \tag{14}$$

The individual elements $R_{pk}-C_{pk}$ with the corresponding time constants $\tau_k = R_{pk}\,C_{pk}$ can then be determined by fitting the depolarization current with the following equations

$$I_{dT}(t) = \sum_{k=1}^{n}\left(A_k e^{\left(\frac{-(t-t_c)}{\tau_k}\right)}\right) \tag{15}$$

where

$$A_k = \frac{V\left(1-e^{\left(\frac{-t_c}{\tau_k}\right)}\right)}{R_{pk}} \tag{16}$$

The modeling process starts with the largest time constant branch. The depolarization current at longer time can be assumed due only to the largest time constant branch, with the influences of the rest of the smaller time constant branches dying down well before that time.

Therefore, the final part of the depolarization current is used to find out the values of τ_k corresponding to the largest time constant branch using an exponential curve fitting technique [9]. Once the exponential component with the largest time constant is identified, it is then subtracted from the depolarization current to go to the next level. In this level, the final part of the resultant current curve is influenced by the second largest time constant only, with the next smaller time constant branches practically going to zero well before that time. Following the same curve fitting technique the value of τ_k corresponding to the second largest time constant branch is identified. The identification of the next R-C branches can be achieved by following the same procedure. Once the values of τ_k corresponding to different time constant branches are identified, the values of R_{pk} and C_{pk} can be easily separated and the equivalent model can be constructed.

5 EXPERIMENTAL SET-UP

New distribution class metal oxide surge arresters of 10 kA ratings used for this study were commercial devices produced by one particular manufacturer. There were two different types of arresters- (i) a double block type labeled D and (ii) a single block type labeled S. The arrester D had rated voltage of 12.5 kV while arrester S consisted only one block and had rated voltage of 6.3 kV. The Experimental procedure is summarized as follows:

5.1 BEFORE DIAGNOSTICS

1. Polarization and depolarization currents were measured with 1000 V_{dc} and polarization and depolarization time was 10^4 s. The measurement circuit diagram is shown in Figure 5.

2. Return voltage measurement (RVM) was performed on all MOSA varistors with 1000 V_{dc}, 200 s charging time and 100 s discharging time. The RVM circuit diagram is shown in Figure 6.

Two terminals of the arresters were short circuited to ground for at least 24 h before the measurement steps 1 and 2 were performed. This was done to eliminate the previous polarization effects (commonly known as memory effects), which normally affect the accuracy of the measurement.

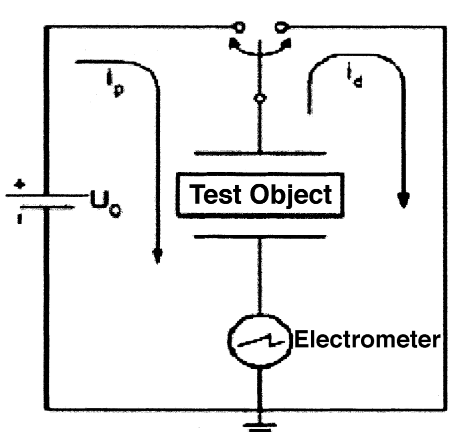

Figure 5. PDC measurement.

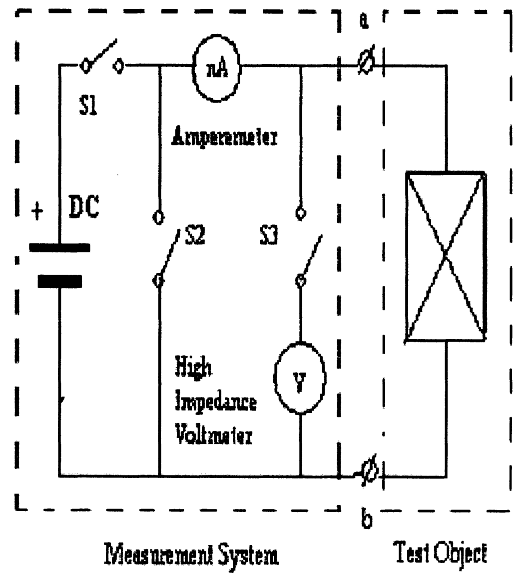

Figure 6. RVM circuit diagram.

5.2 ARTIFICIAL DEGRADATION PROCESSES

All MOSA's were degraded by lightning current impulses. Arresters D and S were subjected to 5 groups of multi-pulse current at 2 p.u. of the rated current with small time intervals required to charge the system. The multi-pulse current test consisted of quintuple (5) 8/20 μs lightning current impulses with a difference of 20-40 ms between each pulse [10].

5.3 AFTER DIAGNOSTICS

Steps 1 and 2 were repeated on the artificially degraded arresters to see the changes and will be referred as "after diagnostic" measurements.

6 POLARIZATION MODEL VALIDATION

The available values from the measured polarization current are the total polarization and depolarization currents with respect to time, insulation resistance R_g (from the difference between polarization and depolarization at larger values of time). The capacitance, C, was measured using a Schering bridge at the power frequency. The relative permittivity, (ϵ_r, at power frequency is typically 10 for ZnO varistor [11] and it was used to calculate geometric capacitance Cg by equation (2)

During the depolarization process the capacitance C_{pk} is discharging through the resistance R_{pk}. Each branch current is modeled by an exponential function as de-

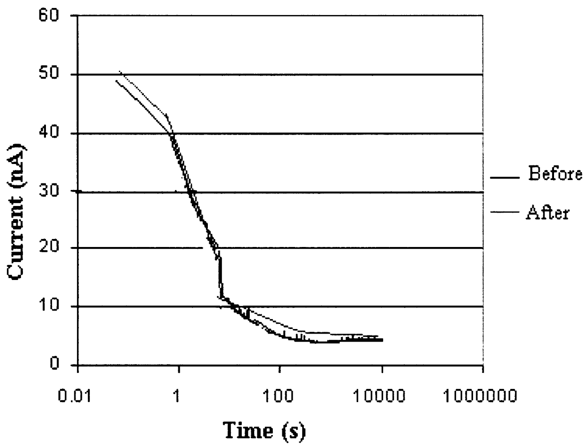

Figure 7. Polarization current measurements on arrester S for before and after application of lightning current impulses.

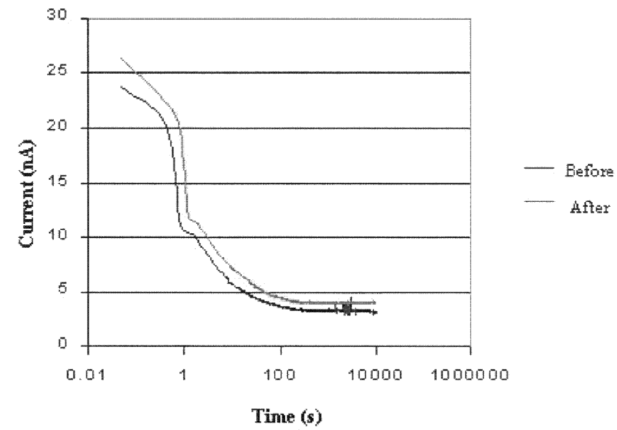

Figure 9. Polarization current measurements on arrester D for before and after application of lightning current impulses.

scribed in equation (13). The software starts calculation at the largest time constant. In Figure 7, x axis is time in logarithmic scale and y axis is in linear scale. A straight line is fitted with the last few points of the measured depolarization current data. The slope of the line is calculated from the fitted straight line. Once the slope is calculated from equations (17) and (18), equations (16) and (18) can be used to calculate R_{pk} and C_{pk}.

The slope of depolarization current between last two selected points $t_d = t_1$ and $t_d = t_2$, can be calculated by equations (17) and (18)

$$\begin{aligned} & ln[I_{dT}(t_2)] - ln[I_{dT}(t_1)] \\ & = ln\left[\sum_{k=1}^{n} I_{dk}(t_2)\right] - 1n\left[\sum_{k=1}^{n} I_{dk}(t_1)\right] \\ & \cong ln\left[\frac{V_{cpk}\exp\left(\frac{-t_1}{\tau_k}\right)}{R_k}\right] - ln\left[\frac{V_{cpk}\exp\left(\frac{-t_2}{\tau_k}\right)}{R_k}\right] \end{aligned} \tag{17}$$

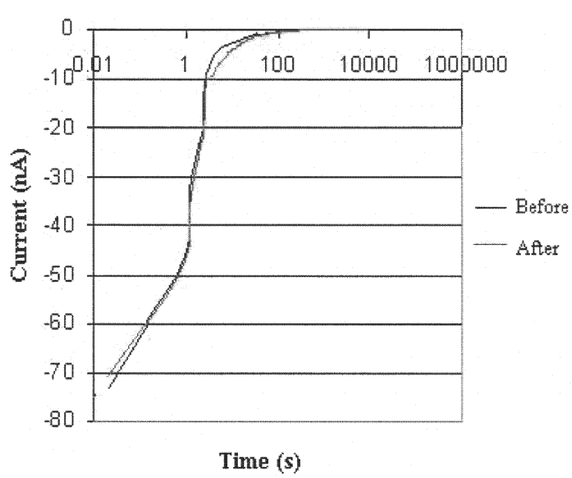

Figure 8. Depolarization currents on arrester S for before and after application of lightning current impulses.

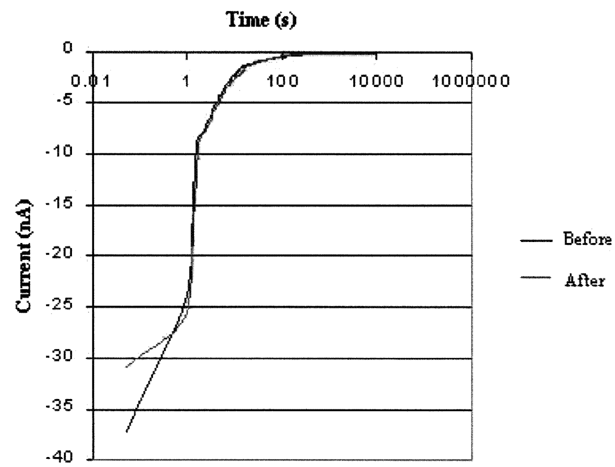

Figure 10. Depolarization current measurements on arrester D for before and after application of lightning current impulses.

$$\therefore slope \cong R_{pk}C_{pk} \cong \frac{t_2 - t_1}{ln[I_{dT}(t_2)] - 1n[I_{dT}(t_1)]} \tag{18}$$

where $0 < t_2 < t_1 < 10000$ s.

First the values of R-C's are estimated from the simulation methodology as described in this section and then polarization/depolarization current was simulated based on these simulated circuit parameters. Finally, the validation was performed by comparing the measurement results of the polarization/depolarization current curves and the simulation results of the polarization model.

Polarization/depolarization currents of S and D arresters are plotted in Figures 7, 8 and 9 and 10, respectively for before and after application of lightning current impulses. The polarization models (before and after the application of lightning current impulses) showed good accuracies compared to the measurement results at the long constant polarization and depolarization stages. Both Figures 11 and 12 show that the arrester S polarization models before and after the application of lightning im-

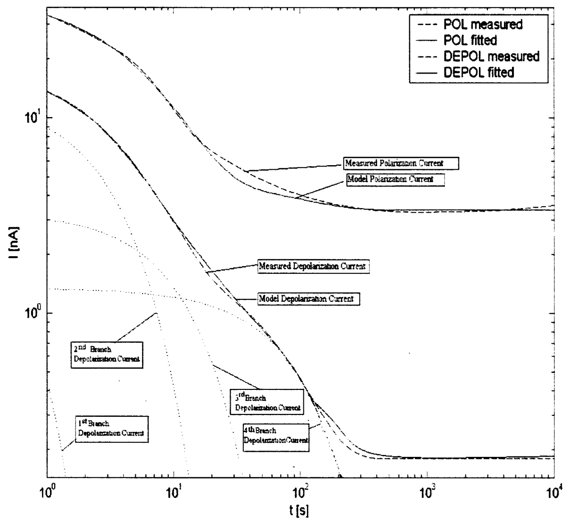

Figure 11. Comparison of measured polarization/depolarization current on arrester S before the application of lightning current impulses.

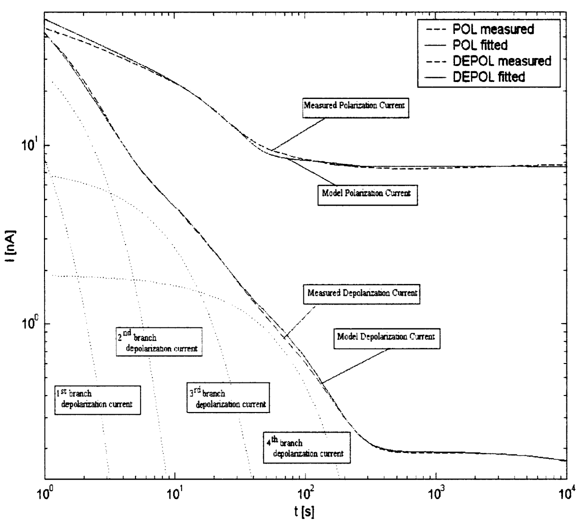

Figure 12. Comparison of measured polarization/depolarization current on arrester S after the application of lightning current impulses.

pulses; consist of 4 polarization branches with each branch having different time constants. Table 1 compares the model parameters before and after the application of lightning current impulses.

The comparisons of the model parameters showed that the insulation resistance (R_g) and branch resistances (R_{p1} − R_{p3}) reduced while the geometric capacitance (C_g) and branch capacitances (C_{p1} − C_{p4}) increased after the application of lightning current impulses. These results suggest that the insulation condition of arrester S have degraded by lowering its insulation resistance and increasing its capacitances. These would increase the leakage current during MOSA's normal operation.

The polarization model was also simulated on arrester D before and after the application of lightning current impulses. The comparisons of simulation results to the actual polarization/depolarization current curves on arrester D are shown in Figures 13 and 14.

Both Figures 13 and 14 showed that the simulation results showed good comparisons with the measured polarization/depolarization current on arrester D. The arrester D polarization models before and after the application of lightning impulses consist of 4 polarization branches with each branch having a different time constant. Arrester D model parameters before and after the application of lightning current impulses are given in Table 2.

The arrester D polarization model parameters showed that the geometric capacitance and branch capacitances (C_{p1} to C_{p4}) increased after the application of lightning current impulses. Meanwhile, the insulation resistance (R_g) and branch resistances (R_{p1} to R_{p4}) are all reduced. This might indicate that arrester D has degraded after the application of lightning current impulses by lowering its insulation resistance.

Table 1. Polarization model parameters for arrester S before and after application of lightning current impulses.

	Before	After
C_g	1.59×10^{-11} F	1.62×10^{-11} F
R_g	3.09×10^{11} Ω	2.9×10^{11} Ω
R_{p1}	7.45×10^{11} Ω	6.05×10^{11} Ωs
R_{p2}	3.03×10^{11} Ω	1.32×10^{11} Ω
R_{p3}	8.02×10^{10} Ω	1.73×10^{10} Ω
R_{p4}	1.29×10^{11} Ωs	2.01×10^{11} Ωs
C_{p1}	1.25×10^{-10} F	1.33×10^{-11} F
C_{p2}	3.71×10^{-11} F	7.27×10^{-11} F
C_{p3}	3.66×10^{-11} F	$7.28 \times 10^{-11}1$ F
C_{p4}	2.75×10^{-12} F	3.02×10^{-11} F

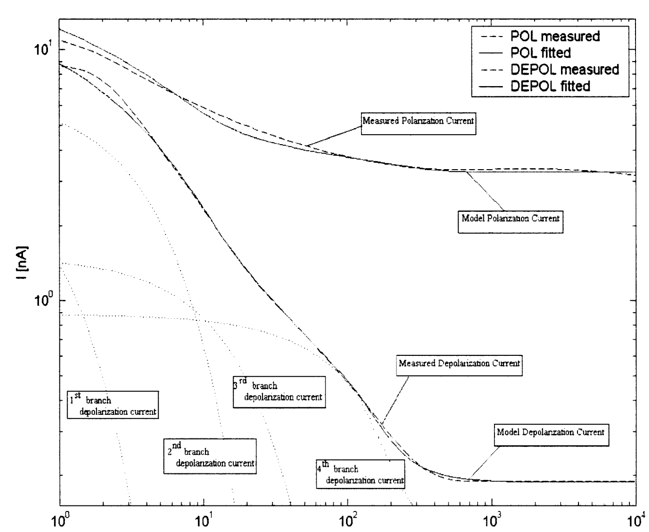

Figure 13. Comparison of measured polarization/depolarization current on arrester D before the Application of Lightning Current Impulses.

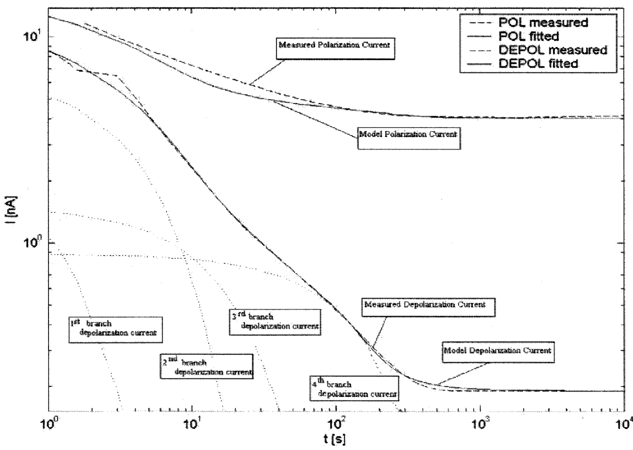

Figure 14. Comparison of measured polarization/depolarization current on arrester D after the application of lightning current impulses.

Table 2. The polarization model parameters for arrester D before and after application of lightning current impulses.

	Before	After
C_g	7.25×10^{-12} F	80.6×10^{-12} F
R_g	5.75×10^{11} Ω	4.03×10^{11} Ω
R_{p1}	1.13×10^{12} Ω	9.87×10^{11} Ω
R_{p2}	6.67×10^{11} Ω	3.67×10^{11} Ω
R_{p3}	1.55×10^{11} Ω	1.05×10^{11} Ω
R_{p4}	2.52×10^{11} Ω	1.91×10^{11} Ω
C_{p1}	1.41×10^{-10} F	1.61×10^{-10} F
C_{p2}	2.63×10^{-11} F	2.83×10^{-11} F
C_{p3}	3.82×10^{-11} F	4.02×10^{-11} F
C_{p4}	3.81×10^{-12} F	4.32×10^{-12} F

7 POLARIZATION MODEL VALIDATION BY RETURN VOLTAGE

To validate the polarization model for arresters S and D before and after the application of current impulses, the return voltage of each arrester was simulated and compared to the measured data. The return voltage can be described mathematically as follows [12]

1. After the application of dc voltage V across the dielectric for pre-selected time t_c (in s), the n-th capacitor C_{pn} is charged to a voltage V_c with final value of

2. $$V_c(t_c) = V\left(1-\exp\left[-t_c/(R_{pn}\,C_{pn})\right]\right) \qquad (19)$$

3. The dielectric is short-circuited for t_d seconds. The ratio of t_d is set to 1/2 of t_c in this study. The remaining voltage in C_{pn} is given by

$$V_{C_{pn}}(t_c,t_d) = V\left(1-\exp\left[\left(-t_c/R_{pp}C_{pn}\right)\right]\right)\times \exp\left[\left(-t_d/R_{pn}C_{pn}\right)\right] \qquad (20)$$

For each pair (t_c,t_d), the voltage in the n-th capacitor V_{Cpn} achieves a different value. The maximum value of V_{Cpn} is achieved when $t_c = \tau_n \ln 3$, where $\tau_n = R_{pn}\,C_{pn}$. This value is obtained by differentiating equation (20) and setting the result equal to zero.

4. As soon as the short circuit is removed, the RV observed will be the resultant of all remaining voltage in all k capacitors. The measured RV corresponds to the voltage across the dielectric given by

$$V_r(t) = \hat{A}_1(t)\left(1-\exp[-t/\tau_1]\right)\left(\exp[-t/2\tau_1]\right) + \ldots + V\hat{A}_n(t)\left(1-\exp\left[(-t/\tau_n)\right]\exp[-t/2\tau_n]\right) \qquad (21)$$

where:

$$A_i(t_p) = A_{i,1}\exp\left[\left(t_{p1}\right)\right] + \ldots + A_{i,k}\exp\left[t_{pn+1}\right)\right]$$

$$A_{i,j} = \frac{k_i}{p_j}\,\frac{\Pi\hat{A}_1(p_j - z_{i,j})}{\Pi\hat{A}_{k\neq j}(p_j - p_k)}$$

$$\mathrm{j,k} = 1,\ldots,\mathrm{n}+1 \qquad \mathrm{i,1} = 1,\ldots,\mathrm{n}$$

In addition, n is the number of polarization branches. In this investigation n = 4 is used since the polarization models for arresters S and D were derived previously which consist of only four polarization branches.

The return voltage simulation of the polarization model was performed using MATLAB by expanding equation (21). The charging voltage is 1000 V_{dc}, t_c = 200 s and t_d = 100 s. Figures 15, 16, 17 and 18 show the comparison between the simulated results and measured RV data on arresters S and D before and after the application of current impulses respectively.

The return voltage simulation results on Figures 15 to 18 show good comparable results to the return voltage results obtained from the measurements. The simulation results are within 6.5% of the measured data. This proves that arresters S and D polarization models derived previously could be used to represent the insulation polarization parameters of arresters S and D.

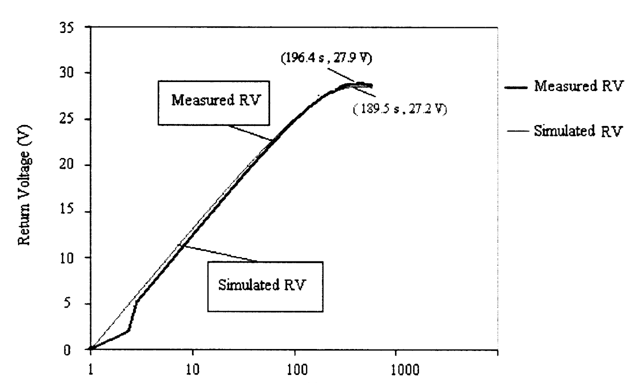

Figure 15. Comparison of return voltage simulation on arrester S polarization model with the measured RV data before the application of current impulses.

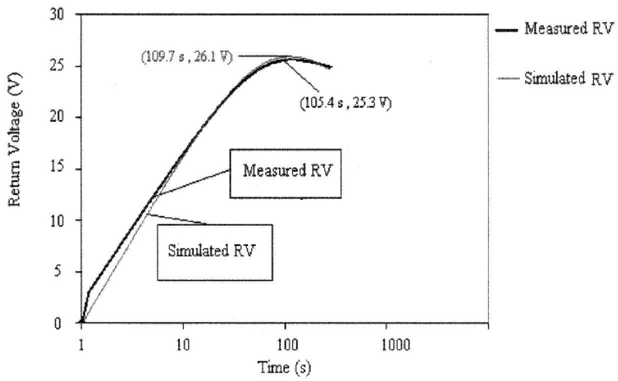

Figure 16. Comparison of return voltage simulation on arrester S polarization model with the measured RV data after the application of current impulses.

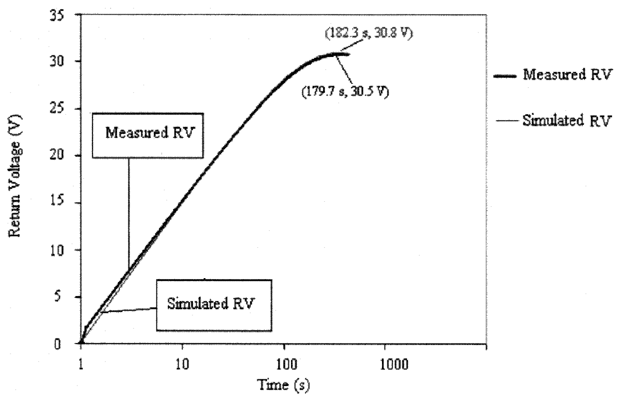

Figure 17. Comparison of return voltage simulation on arrester D polarization model with the measured RV data before the application of current impulses.

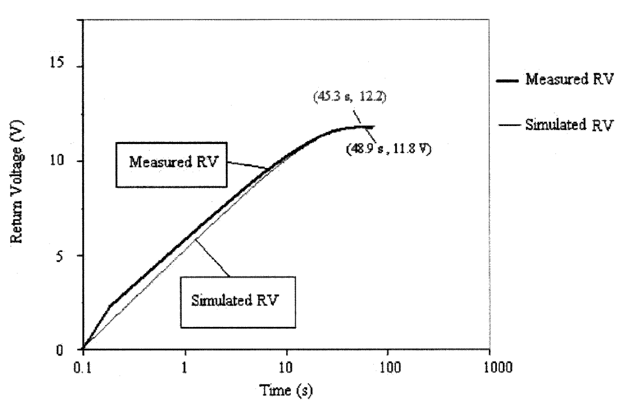

Figure 18. Comparison of return voltage simulation on arrester D polarization model with the measured RV data after the application of current.

8 CONCLUSIONS

In this study, an attempt is made to identify the insulation polarization model of MOSA by means of polarization/depolarization current measurement. The model can be represented by an equivalent model comprising a circuit used to describe dielectric materials with a number of additional R-C branches. The calculation of model parameters is performed and simulated using MATLAB.

The calculated models on arresters S and D before and after the application of lightning current impulses showed a comparable good accuracy to the actual measurement curves (polarization/depolarization currents and return voltage). The comparisons of model parameters indicate that the application of lightning current impulses degrade the arresters by lowering the insulation and branch resistances as well as increasing the geometric and branch capacitances. These would increase the leakage current during arrester's normal operating condition. Therefore, these findings could be useful for the study of the degree of degradation of MOSA after the application of electrical stresses.

This study will be very useful while comparing the circuit parameters of suspected arresters collected from the field with the new ones. Very often field arresters do show clear-cut evidence of pass/fail condition by measuring 1 mA leakage current or lightning impulse residual voltage. However, these tests do not show any evidence of ZnO material degradation under lightning currents. We have previously tested many such arresters with these newer diagnostics and found very important results. A comprehensive mathematical tool like this would provide more information to predict the condition of field arresters in detail. This is under investigation in our current project and will be reported in a future paper.

REFERENCES

[1] K. P. Mardira, T. K. Saha, and R. A. Sutton, "Investigation of Modern Diagnostic Techniques for Metal Oxide Surge Arresters", IEEE Trans. Dielectr. Electr. Insul., Vol. 12, pp. 50–59, 2005.

[2] C. Heinrich and W. Kalkner "Return Voltage Measurement on Metal Oxide Surge Arrester", 10th Intern. Sympos. High Voltage Eng., Vol. 5, pp. 137–40, Montreal, Canada, 1997.

[3] T. K. Saha and T. Dinh, "Return Voltage Measurements on Metal Oxide Surge Arresters", Intern. Sympos. High Voltage Eng., London, UK, Vol. 2, pp. 313–316, 1999.

[4] K. P. Mardira, M. Darveniza and T. K. Saha, "Search for New Diagnostics for Metal Oxide Surge Arrester", IEEE 6th Intern. Conf. Properties and Applications of Dielectric Materials, Xian, China, pp. 947–50, Vol. 2, 2000.

[5] T. K. Saha and P. Purkait, "Investigation of Polarization and Depolarisation Current Measurements for the Assessment of Oil-paper Insulation of Aged Transformers", IEEE Trans. Dielectr. Electr. Insul., Vol. 11, pp. 144–154, 2004.

[6] A. K. Jonscher, *Dielectric Relaxation in Solids*, Chelsea Dielectric Press, London, UK, 1983.

[7] E. Nemeth, "Measuring Voltage Response: a Non Destructive Diagnostic Test Method of High Voltage Insulation", IEE Proc. Sci. Measur. Techn., Vol. 146, pp. 249–252, 1999.

[8] E. Nemeth and T. Horvath, "Fundamental of the Simulation of Dielectric Processes of Insulation", 8th Intern. Sympos. High Voltage Eng., Budapest, Hungary, pp. 177–180, 1993.

[9] T. K. Saha, P. Purkait and F. Müller, "Deriving an Equivalent Circuit of Transformers Insulation for Understanding the Dielectric Response Measurements". *IEEE Transactions on Power Delivery*, Vol. 20, pp. 149–157, 2005.

[10] M. Darveniza, C. J. Andrews, D. R. Mercer and T. M. Parnell, "A Multiple Lightning Impulse Generator", Int. Sympos. High Voltage Eng., New Orleans, paper 47.07, 1989.

[11] L. M. Levinson, and H. R. Philipp, "Application and Characterisation of ZnO Varistors", in *Ceramic Materials for Electronics - Processing, Properties and Applications* (Duchanan, R. C. ed, Marcel Dekker Inc, New York) pp. 375–402, 1986.

[12] P. R. S. Jota, S. M. Islam, and F. G. Jota, "Modeling the Polarization Spectrum in Composite Oil/Paper Insulation Systems", IEEE Trans. Dielectr. Electr. Insul., Vol. 6, pp. 146–151, 1999.

Tapan Kumar Saha (M'93-SM'97) was born in Dhaka, Bangladesh in 1959 and immigrated to Australia in 1989. He received the B.Sc. Engineering (electrical and electronic) degree in 1982 from the Bangladesh University of Engineering & Technology, Dhaka, Bangladesh, the M. Tech. (electrical engineering) degree in 1985 from the Indian Institute of Technology, New Delhi, India and the Ph.D. degree in 1994 from the University of Queensland, Brisbane, Australia. Before joining the University of Queensland as a Lecturer in 1996, he taught at the Bangladesh University of Engineering and Technology, Dhaka, Bangladesh for three and a half years and at James Cook University, Townsville, Australia for two and a half years. Dr Saha is currently a Professor in the School of Information Technology and Electrical Engineering, University of Queensland, Australia. He is a Fellow of the Institution of Engineers, Australia. His research interests include condition monitoring of electrical plants, power systems and power quality.

Karl Primardi Mardira was born in 1976 in Indonesia. He graduated with a B.Eng. (Honours) degree in electrical engineering from the University of Queensland in 1998. In 2003, he completed his Ph.D. degree at the University of Queensland, Australia. His research interests are in power system analysis, power system protection, insulation systems and network grounding.